KOH-MODIFIED DURIAN PEEL BIOCHAR FOR ENHANCED REMOVAL OF SYNTHETIC DYES FROM AQUEOUS ENVIRONMENT

NGUYỄN THÁI ANH[1,2], PHẠM NHƯ NGỌC[1,2], NGUYỄN UYÊN LẬP PHÁT[1,2], ĐẶNG VŨ BÍCH HẠNH[1,2,*]

[1] *Ho Chi Minh City University of Technology (HCMUT)*

[2] *Vietnam National University Ho Chi Minh City*

Abstract

Large quantities of durian peel residues are produced as by-products of consumption and processing, creating a challenge for sustainable waste management. The production of synthetic dyes is on the increase due to their high demand, most especially in the textile and clothing industries. These chemicals (dyes) are massively produced annually in thousands of tons worldwide. Specifically, the annual industrial production of dye compounds is ~ 7x105 tons (Katheresan et al., 2018). A few examples of synthetic dyes are aniline blue, alcian blue, basic fuchsin, methylene blue, crystal violet, toluidine blue, and congo red. Synthetic dyes remain in the physical environment since most of them are difficult to biodegrade and are not usually eliminated during the conventional water treatment processes. Therefore, they cause persistent pollution and ecological risks in aquatic environments. Methylene blue (MB), a representative cationic dye widely used in textile and printing industries, was selected in this study as a model pollutant because of its high stability, intense coloration, and toxicity even at low concentrations.

In this study, durian husk was valorized into biochar and applied as an adsorbent for methylene blue (MB) removal from aqueous solution. The production process was systematically optimized with respect to pyrolysis temperature and residence time. Preliminary tests revealed that biochar prepared at 600°C exhibited markedly higher decolorization efficiency compared with those obtained at 400 and 500°C. Further investigation showed that extending the residence time from 3 to 5 hours enhanced adsorption performance, with the 600°C 5-hour biochar demonstrating the best results. Subsequently, a saponification pretreatment using 5% KOH, with immersion times, the optimized material achieved a maximum MB removal efficiency of approximately 98% and an equilibrium adsorption capacity of about 8.9 mg.g^{-1}. Overall, these results highlight the potential of durian peel biochar, especially after KOH saponification, as a cost-effective and eco-friendly adsorbent for dye-contaminated wastewater.

Keyword: *Biochar, durian husk, KOH saponification, methylene blue, adsorption, wastewater treatment.*

JEL Classification: *Q53, Q55, Q25.*

Received: *15th August 2025****; Revised:*** *7th September 2025; **Accepted:** 20th September 2025.*

1. INTRODUCTION

In recent years, rapid urbanization, industrial expansion, climate change, and upstream alterations in river flow have significantly deteriorated water quality in many regions, particularly within the Mekong Delta (Doan et al., 2025). Increasing discharges of organic matter, nutrients, and synthetic dyes from industrial and domestic activities have raised serious concerns regarding aquatic pollution, with profound risks to both human health and ecosystem integrity. In response to these challenges, sustainable and low-cost adsorbents have attracted considerable attention for wastewater treatment. Among them, biochar has emerged as a promising candidate owing to its unique properties, as it not only valorizes abundant agricultural by-products but also offers a renewable, economical, and environmentally friendly option for contaminant removal.

Biochar is a stable, highly aromatic, carbon-rich porous material produced through the pyrolysis of biomass (e.g., crop residues, livestock, and poultry manure) under anaerobic or oxygen-limited conditions, and it generally exhibits alkaline characteristics under natural environments (Xu et al., 2017). As an organic amendment, biochar can not only modify the physical and chemical properties of soils but also demonstrates strong adsorption capacity owing to its large specific surface area and well-developed pore structure. Consequently, it has attracted increasing attention in recent years for applications in carbon sequestration, soil improvement, pollution control, and other environmental management practices (Sakhiya et al., 2020b; Ravindiran et al., 2024). The adsorption of pollutants by biochar is influenced by multiple factors, among which its intrinsic characteristics, such as pore size distribution and types of surface

functional groups, play decisive roles (Oliveira et al., 2017). Numerous studies have highlighted that the pyrolysis temperature significantly alters the specific surface area, pore architecture, surface functionalities, and aromaticity of biochar, thereby modulating its adsorption efficiency toward various contaminants (Raj et al., 2021b; P. Zhang et al., 2019b). For instance, G.Zhang et al. (2011) reported that biochar prepared at higher temperatures exhibited a greater degree of aromatization, larger surface area, more complete pore structure, reduced abundance of polar surface groups, and enhanced adsorption capacity for simazine.

The environmental burden of industrial wastewater from textile manufacturing is substantial, as it is characterized by high concentrations of auxiliary chemicals, heavy metals, and dyes. This effluent is a significant contributor to water degradation, with the dyeing and finishing phase alone accounting for approximately 20% of all pollution in clean water sources. The composition of textile dyeing wastewater includes high concentrations of recalcitrant organic molecules, notably synthetic dyes like indigo blue and indigo carmine, which are chemically stable and difficult to degrade (Yaseen & Scholz, 2018). Furthermore, the effluent's toxicity is intensified by the presence of heavy metals, including chromium, copper, zinc, and lead, which are employed to fix dyes. This poses a risk to both human health, daily life and the aqueous environment, including the potential for skin irritation and carcinogenic effects. In order to alleviate this issue, numerous sophisticated treatment technologies have been implemented. Ozone oxidation has demonstrated significant potential for the purification of textile wastewater, and the efficacy of COD and color removal has been enhanced through the integration of AOPs or UV treatment with coagulation pretreatment.

MB is extensively used for dyeing fabrics, papers, and leathers in textile and garment industries, leading to the discharge of large volumes of dye-laden effluents into aquatic environments. According to Oladoye et al. (2022), MB poses ecological and health risks owing to its monoamine-oxidase inhibitory properties that can induce serotonin toxicity in humans at doses above 5 $mg.kg^{-1}$. Its complex aromatic and heterocyclic structure renders it highly resistant to biodegradation, oxidation, and even photolysis (Shahinyan et al., 2019), allowing persistence in water bodies where it reduces light penetration and disrupts aquatic ecosystems. Consequently, the effective removal of MB from wastewater is of critical environmental significance. The adsorption of MB onto biochar occurs through a combination of physicochemical mechanisms, including electrostatic attraction between MB^+ cations and negatively charged oxygen-containing groups, ion exchange with alkali or alkaline-earth cations (K^+, Ca^{2+}, Mg^{2+}), π–π stacking between aromatic domains, π–cation interactions, and hydrogen bonding (Xu et al., 2017; Sakhiya et al., 2020). Owing to its well-defined structure, planar geometry (~1.4 × 0.6 × 0.4 nm), and strong absorption peak at 664–665 nm, MB is widely used as a benchmark molecule to probe adsorption pathways and evaluate biochar performance, offering mechanistic insights relevant to a broader range of persistent organic pollutants and heavy metals.

Vietnam has emerged as one of Southeast Asia's leading durian producers, driven by strong domestic demand and booming exports, particularly to China. In 2023, the country's durian cultivation area exceeded 110,000 hectares, producing over 850,000 tons of fruit and generating export revenues surpassing 2.1 billion USD (Khanh, 2025). However, alongside this impressive growth lies a pressing environmental challenge. Structurally, durian fruit comprises three main parts: the edible aril (20–35% of total weight), the seeds (5–15%), and the husk, which constitutes the majority fraction at 55–66% (Nordin et al., 2017). Consequently, most of the durian biomass remains as an underutilized by-product. With the sharp rise in production, husk disposal has become a serious concern. For instance, durian farming in the Philippines generates over 22,000 tons of husks annually (Phoung, 2012), while in Vietnam, the figure exceeded 150,000 tons in 2023 and is projected to reach 300.000–450.000 tons in the near future (Khanh, 2025). Current disposal practices are largely unsustainable, as the husks are often dumped into landfills or left to decompose in open areas, releasing unpleasant odors, attracting pests, and emitting methane (CH_4), a greenhouse gas with a global warming potential 25 times greater than CO_2, thereby compounding the environmental burden of the durian industry.

From the perspective of a circular economy, the valorization of durian husk waste presents a promising pathway for sustainable waste management. Compared with other agricultural residues, durian husk offers both economic and technical advantages. It is abundantly available and has an extremely low market value, while its composition, rich in cellulose, hemicellulose, and lignin, makes it particularly suitable for thermochemical conversion into biochar. In contrast, other residues such as bamboo and coconut shells are often repurposed for higher-value applications (e.g., handicrafts, paper, or organic fertilizers), leaving durian husk as a low-cost yet underexploited feedstock

ideal for developing biochar-based adsorbents within a circular economy framework.

Building upon this context, the present study evaluates the adsorption performance of biochar prepared (i) at 400, 500, and 600°C for a fixed residence time of 4 h; (ii) at 600°C with varied residence times of 3, 4, and 5 h to identify the optimal duration; and (iii) with KOH pretreatment under the optimal condition compared with its non-pretreated counterpart.

2. MATERIALS AND METHODS

2.1. Materials and chemicals

Durian husks were collected from local markets, thoroughly washed to remove impurities, and oven-dried for further use. Methylene Blue (MB, 82% purity), potassium hydroxide (KOH, 5% solution), and distilled water were employed as chemical reagents.

2.2. Preparation

In the preliminary optimization stage, durian husks were pyrolyzed at different temperatures (400, 500, and 600°C) under fixed residence time conditions. The results indicated that biochar obtained at 600°C exhibited superior performance compared to lower pyrolysis temperatures. At the selected temperature of 600°C, residence times of 3, 4, and 5 hours were further evaluated, and 5 hours was found to be optimal.

For chemical pretreatment, the husks were immersed in 5% KOH solution for 30 minutes, lightly rinsed with distilled water, oven-dried, and subsequently pyrolyzed at 600°C for 5 hours.

2.3. Sample names

C 400/500/600 : Biochar (without KOH) produced at 400/500/600°C with fixed residence time.

C600-3/4/5 : Biochar is produced at 600°C for 3/4/5 hours, respectively.

C306005 : Biochar pretreated with 5% KOH for 30 minutes, then pyrolyzed at 600°C for 5 hours.

2.4. Adsorption experiment

2.4.1. Adsorption dynamics experiment

Batch adsorption experiments were conducted to investigate the adsorption dynamics of methylene blue (MB) onto the prepared biochar samples. A fixed amount of biochar (0.50 g) was added into MB aqueous solutions of known initial concentration (C_0 = 100 mg.L^{-1}, V = 45 mL). The mixtures were agitated in an orbital shaker at a constant speed of 120 rpm (ambient temperature, 28°C, pH ≈ 10). At predetermined time intervals, aliquots were withdrawn, filtered, and analyzed for the residual MB concentration using a UV-Vis spectrophotometer at λ = 664 nm.

The adsorption capacity (q_t, mg.g^{-1}) at time t was calculated according to:

$$q_t = \frac{(C_0 - C_t) \times V}{m}$$

where: C_0 and C_t are the initial and residual dye concentrations (mg.L^{-1}), respectively, V is the solution volume (L), and m is the adsorbent mass (g).

The adsorption kinetic experimental data were fitted and analyzed using the Pseudo-first-order (PFO), Pseudo-second-order (PSO), and Intra-particle diffusion (IPD) models. The corresponding linearized equations are presented below:

Pseudo-first-order (PFO):

$$\ln(q_e - q_t) = \ln q_e - k_1 t$$

Where: q_e (mg.g^{-1}) and qt (mg.g^{-1}) are the adsorption capacities at equilibrium and at time t (min), respectively, and k_1 (min-1) is the rate constant of the PFO model.

Pseudo-second-order (PSO):

$$\frac{t}{q_t} = \frac{1}{k_2 q_e^2} + \frac{t}{q_e}$$

Where: k_2 (g.mg-1.min-1) is the rate constant of the PSO model.

Intra-particle diffusion (IPD):

$$q_t = k_i t^{0.5} + C$$

Where: k_i (mg.g^{-1}.min$^{-1/2}$) is the intra-particle diffusion rate constant, and C reflects the boundary layer thickness.

2.4.2 Isothermal adsorption experiment

Equilibrium adsorption isotherm studies were carried out by contacting a fixed mass of biochar (0.50 g) with MB solutions of varying initial concentrations (C_0 = 20-200 mg.L^{-1}) at a constant volume (45 mL) and pH (≈10). The suspensions were shaken at 150 rpm and 28°C until adsorption equilibrium was attained (after 180 min, as determined from the kinetic experiments). The supernatants were filtered, and the residual MB concentrations were measured using a UV-Vis spectrophotometer at 664 nm.

The equilibrium adsorption capacity (q_e, mg.g^{-1}) was calculated according to:

$$q_e = \frac{(C_0 - C_e) \times V}{m}$$

Where: C_0 and C_e are the initial and equilibrium dye concentrations (mg.L^{-1}), respectively; V is the solution volume (L), and m is the adsorbent mass (g).

The isothermal adsorption experimental data were fitted and analyzed using the Langmuir, Freundlich, and Temkin models. The linearized forms of the equations are expressed as:

Langmuir model:

$$q_e = \frac{q_{max} K_L C_e}{1 + K_L C_e}$$

Where qe (mg.g^{-1}) is the adsorption capacity at equilibrium

and C_e ($mg.L^{-1}$) is the equilibrium concentration. q_{max} ($mg.g^{-1}$) represents the maximum adsorption capacity; K_L ($L.mg^{-1}$) is the Langmuir adsorption constant;

Freundlich model:

$$q_e = K_F C_e^{\frac{1}{n}}$$

Where K_F[$(mg.g^{-1})(L.mg^{-1})^{-1/n}$] is the Freundlich constant; n is the Freundlich heterogeneity factor.

3. RESULTS AND DISCUSSION

3.1. Initial properties and Preliminary optimization

The preliminary experiments were conducted to evaluate the effect of pyrolysis temperature and residence time on the adsorption performance of the biochar toward methylene blue (MB).

Figure 1 illustrates the integrated effect of pyrolysis temperature (400, 500, and 600°C) and residence time (3, 4, and 5 hours) on the MB removal efficiency of biochar. The removal percentage increased substantially with temperature, reaching more than 98% at 500°C and nearly complete removal at 600°C. This improvement would be due to catalyzing the decomposition of such compounds as well as generating more stable aromatic carbon structures. This trend is consistent with previous findings for MS and SG. The observed increases in surface area and pore volume are attributed to the thermal degradation of organic components such as hemicellulose, cellulose, and lignin, along with the development of vascular bundles or channel-like structures during pyrolysis (Kim et al., 2013; Li et al., 2012). According to Lee et al., 2013, cellulose and hemicellulose in MS begin to decompose around 500°C. When the pyrolysis temperature rises above 500°C, the breakdown of hemicellulose and other organics promotes the generation of additional micropores in biochar (Jeong et al., 2015). Furthermore, the decomposition of lignin accompanied by the rapid release of H_2 and CH_4 leads to a marked increase in surface area and pore volume between 500 and 600°C. In addition, extending the residence time from 3 to 5 hours at 600°C enhanced MB removal, with

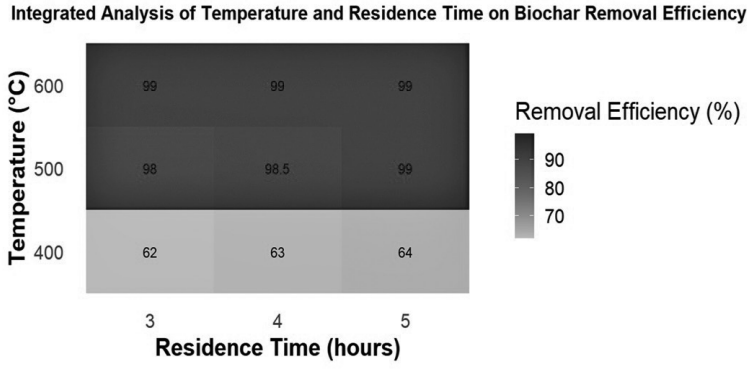

Figure 1. Integrated effect of pyrolysis temperature and residence time on MB removal efficiency of biochar

optimal performance (~98%) achieved after 5 hours. The slight increase can be attributed to the reduction of volatile matter and the increase of fixed carbon, along with higher surface pH and a greater abundance of basic functional groups, which provide more favorable adsorption sites. However, after about 4 to 5 hours, the structure and surface properties of the biochar became nearly stabilized, resulting in only a minor improvement and a tendency to level off (Sun et al., 2016).Therefore, a residence time of 5 hours was selected as the optimal condition to ensure high and stable adsorption performance.

3.2. Effect of KOH

Analysis results indicated that the addition of KOH altered the composition of the biochar. In terms of ash content, the untreated sample exhibited a markedly higher value of about 25%, whereas the KOH-saponified sample showed a reduced level of approximately 10%. Moreover, the moisture content decreased significantly during dry storage and under high-temperature conditions, and water retention was further diminished after KOH modification compared to the initial state. In contrast, KOH reacts with the carbon network through activation processes, leading to the consumption of carbon and a subsequent decline in its content (Wahyu et al., 2025). In addition, biochar activated with KOH solution exhibited higher values in cation exchange capacity (CEC), which is also dependent on the biomass feedstock and pyrolysis conditions (Loc et al., 2018). With the increase of pH from 10 to nearly 14, the removal efficiency of MB rose significantly, reaching its maximum at pH 13.5. According to Gurav et al. (2021), as the pH value increases, the electrostatic attraction between the negatively charged biochar surface and the cationic dye MB^+ becomes stronger, resulting in a higher adsorption capacity.

The comparison of non-activated and activated biochars reveals a clear difference in removal efficiency. Activated biochars exhibited an increase from 90.5–91.7% to over 98% compared with the non-activated sample. This improvement is attributed to the greater number of active-binding sites generated on the surface after chemical modification, together with the formation of new functional groups and enhanced ion-exchange properties that facilitate adsorption.

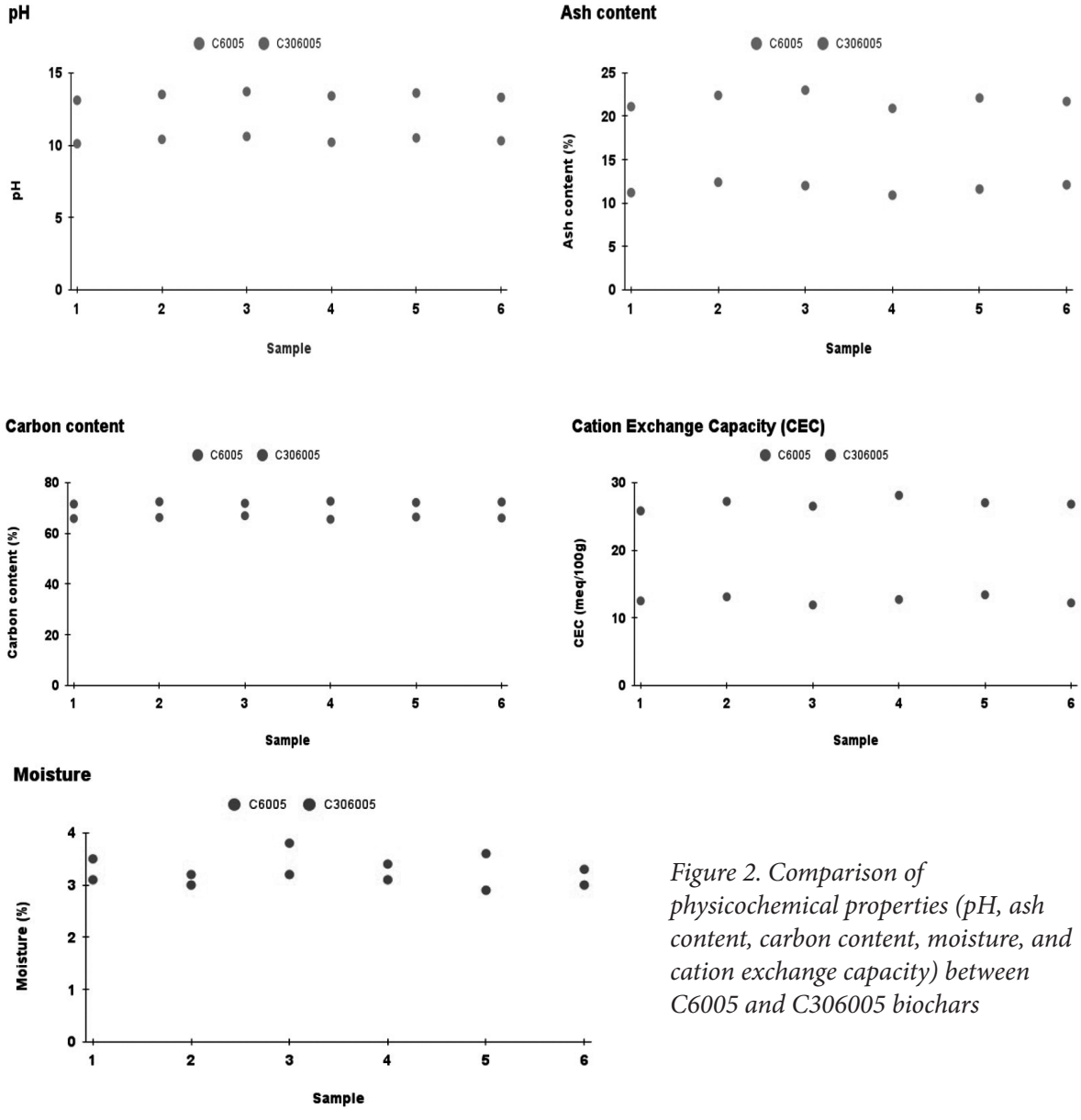

Figure 2. Comparison of physicochemical properties (pH, ash content, carbon content, moisture, and cation exchange capacity) between C6005 and C306005 biochars

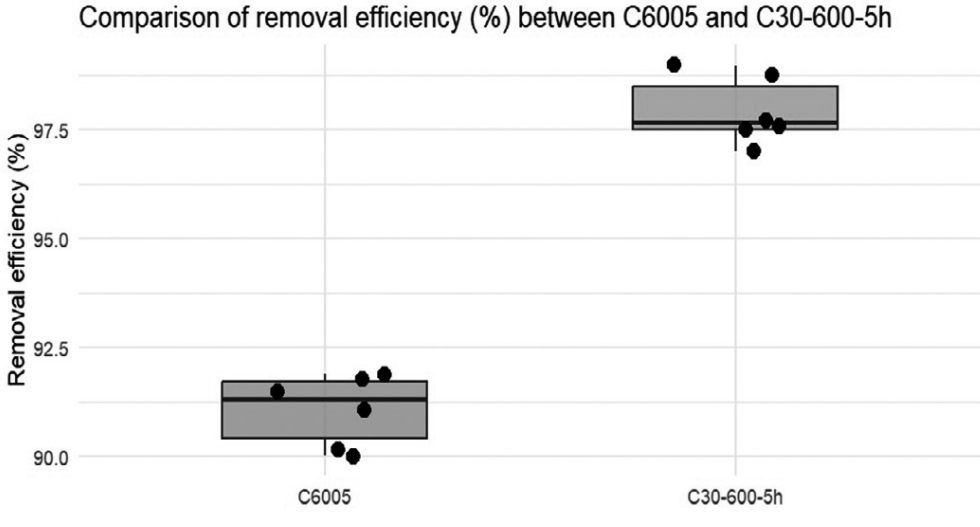

Figure 3. Comparison of removal efficiency (%) between C6005 and C306005

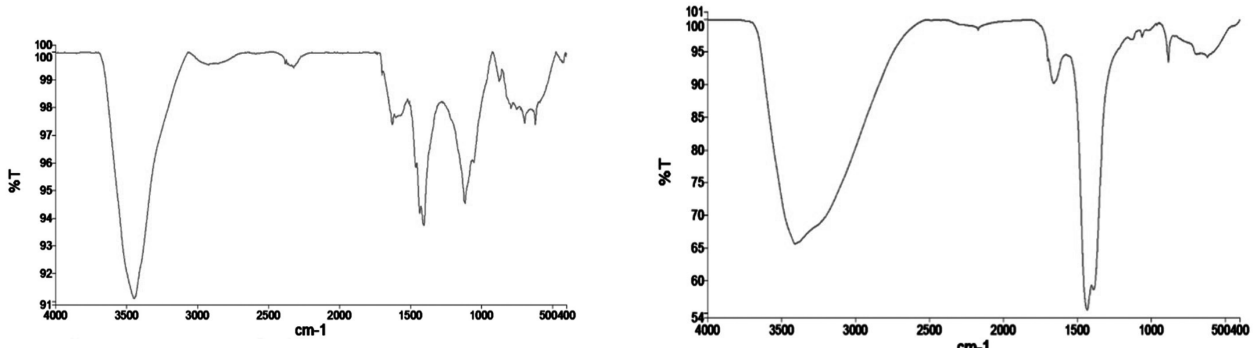

Figure 4. FTIR spectra of biochars: (a) C6005 and (b) C306005

3.3. Material properties

The FTIR spectra of the two biochars reveal clear structural differences between the C6005 and C306005. In C6005, weak aliphatic C–H stretching vibrations at 2960, 2926, and 2852 cm^{-1} are still detectable, suggesting the persistence of residual hydrocarbon chains, while the absorption band at 1700–1627 cm^{-1} corresponds to C=O and aromatic C=C groups. Several out-of-plane bending vibrations of aromatic C–H are observed at 893, 872, 789, and 748 cm^{-1}, together with signals below 600 cm^{-1} attributed to Si–O or metal–O bonds, reflecting the contribution of mineral phases. By contrast, the spectrum of C306005 is dominated by a broad O–H stretching band at 3346 cm^{-1}, accompanied by the disappearance of aliphatic C–H peaks, indicating a more complete carbonization process. A distinct absorption at 1432 cm^{-1}, along with additional bands at 1389 and 1329 cm^{-1}, is assigned to CO_3^{2-} vibrations, confirming the presence of surface carbonate after KOH pretreatment. Strong absorptions at 1248 and 1136 cm^{-1} are related to C–O stretching of phenolic and ether groups, while the peaks at 836 and 816 cm^{-1} further confirm the aromatic backbone of the biochar. Overall, C6005 retains some aliphatic and carbonyl functionalities and shows a stronger contribution from mineral phases, whereas C306005 exhibits a more stable aromatic framework enriched with hydroxyl and carbonate groups. These modifications render the surface more alkaline and polar, thereby increasing the

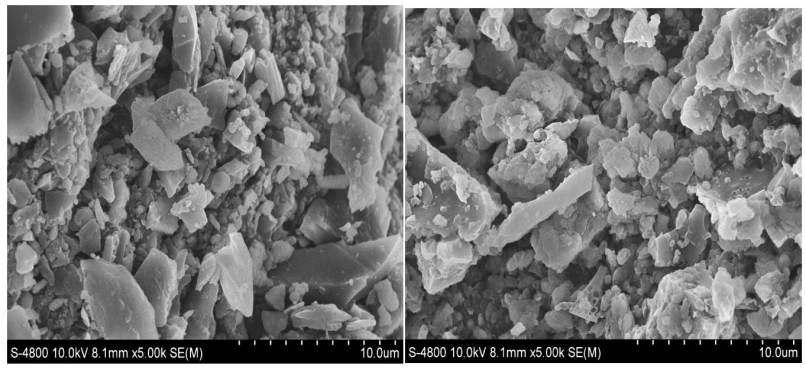

Figure 5. SEM images of (a) C6005 and (b) C306005

number of active adsorption sites and facilitating multiple adsorption mechanisms, including electrostatic interactions with cationic MB, hydrogen bonding with hydroxyl functionalities, and π–π interactions between the aromatic rings of the biochar and the dye.

The SEM micrographs recorded at 10 kV and ×5000 magnification reveal clear morphological differences between C6005 and C306005. The pristine C6005 sample Figure 5a exhibits a relatively compact surface structure with stacked plate-like particles and limited pore development. In contrast, the KOH-pretreated C306005 Figure 5b shows a rougher texture with extensive fragmentation, micro-cracks, and a higher density of cavities. This structural transformation can be attributed to the alkaline saponification process, during which KOH penetrates the biomass matrix and reacts with hemicellulose and lignin, promoting partial dissolution of inorganic components and weakening the carbon framework, resulting in the formation of a well-developed porous structure on the biochar surface, with a predominance of micropores and the appearance of active functional groups (Ding & Liu, 2020; Jedynak & Charmas, 2023). The internal components of the biomass are revealed, and a uniform chemical reaction is facilitated by the presence of KOH, which is highly effective. Subsequent pyrolysis further enhances the release of volatile matter, leaving behind a more disordered and porous network.

3.4. Kinetic and adsorption isotherm

The kinetic parameters of MB adsorption onto C6005 and C306005 are summarized in Table 1. For C6005, the PSO model provided a better fit (R^2 = 0.9993; qe,cal close to qe,exp, suggesting

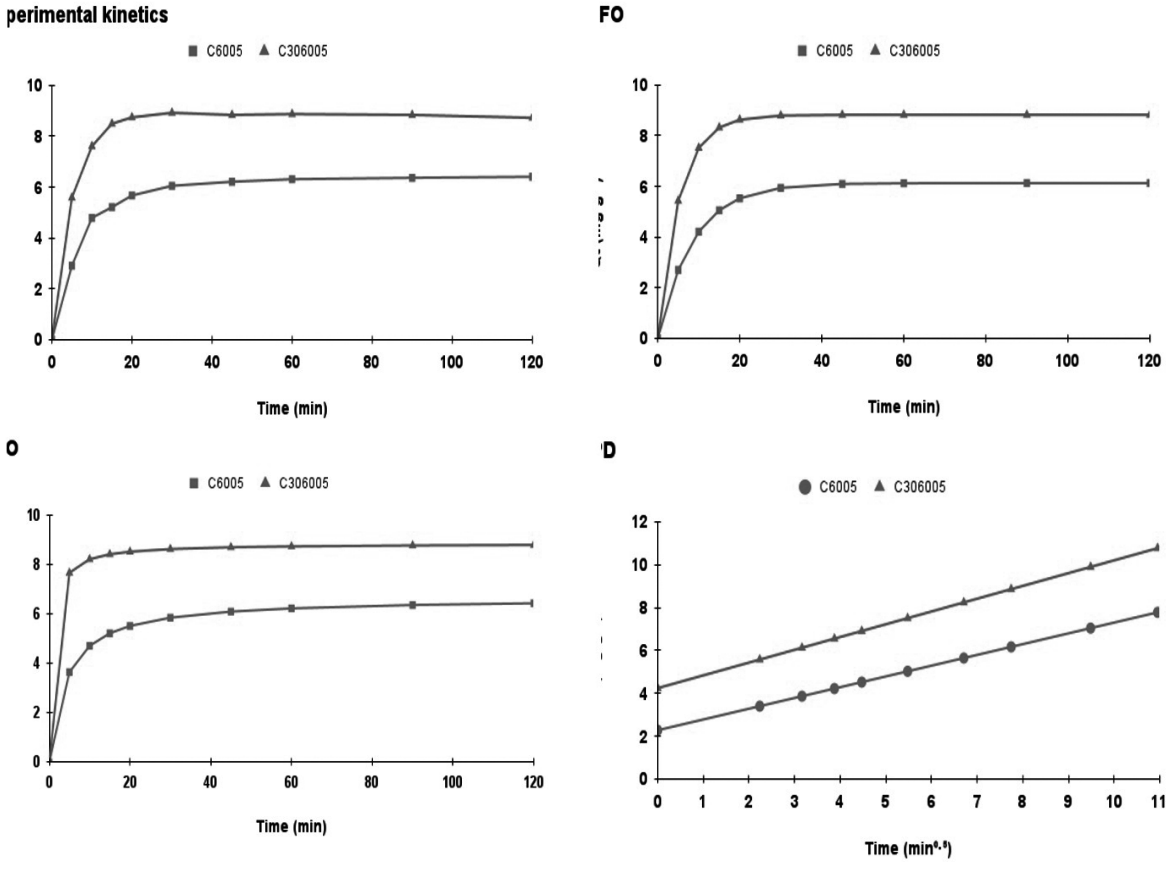

Figure 6. Adsorption kinetics of methylene blue onto C6005 and C306005 biochars: (a) experimental data, (b) pseudo-first-order (PFO) model, (c) pseudo-second-order (PSO) model, and (d) intra-particle diffusion (IPD) model.

Table 1. Parameters k_1, k_2, q_e, R^2, RMSE

Sample	Model	k_1(1/min)	k_2(g.mg^{-1}.min^{-1})	q_e, exp	q_e, cal	R^2	RMSE
C6005	PFO	0.1162		6.4050	6.1275	0.9749	0.2489
	PSO		0.0364	6.4050	6.6684	0.9993	0.2512
C306005	PFO	0.1912		8.9200	8.8206	0.9998	0.1014
	PSO		0.0364	8.9200	8.8648	0.9993	0.7035

that the adsorption process is mainly governed by chemical interactions (chemisorption) between MB and surface functional groups.

In contrast, for C306005, the PFO model showed superior agreement (with a markedly lower RMSE), which is typically observed when adsorption kinetics are dominated by film or intraparticle diffusion and physical adsorption. The biochar treated at 600 °C for 5 hours with alkali pretreatment exhibited increased surface area and porosity, suggesting that adsorption is primarily governed by rapid diffusion and pore-filling mechanisms. Furthermore, the superior fit of the Freundlich isotherm compared to the Langmuir model indicates the heterogeneous nature of the surface, thereby reinforcing the suitability of the PFO model for describing the kinetics, while not excluding the contribution of electrostatic and π–π interactions.

The isotherm parameters of MB adsorption onto C6005 and C30-600-5h are summarized in Table 2. For C6005, the Langmuir model exhibited a higher correlation coefficient and lower RMSE, with the calculatedq_{max} being close to the experimental value, indicating that adsorption primarily occurred on a homogeneous surface through monolayer coverage. In contrast, for C306005, the Freundlich model provided a better fit, reflecting the heterogeneous surface characteristics of the modified biochar. This suggests that adsorption on C306005 is governed by multiple

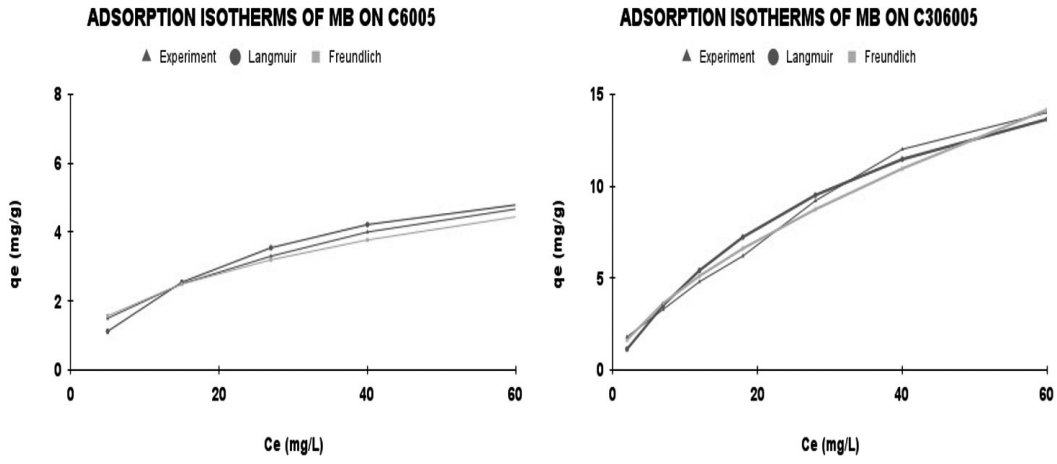

Figure 7. Adsorption isotherms of MB on C6005 and C306005: experimental data and model fittings

Table 2. Parameters of q_{max}, K_L, K_F, n, R^2, RMSE

Sample	Model	q_{max} ($mg.g^{-1}$)	K_L(L/mg)	K_F	n	R^2	RMSE
C6005	Langmuir	6.9582	0.0384			0.9928	0.2000
	Freundlich			0.7976	2.3743	0.9907	0.2069
C306005	Langmuir	21.9921	0.0272			0.8757	0.5903
	Freundlich			1.0603	1.5799	0.9887	0.4979

active sites with a pore-filling mechanism, while electrostatic and π–π interactions may also contribute.

The electrostatic attraction is the force of attraction or repulsion between two charged particles, which is also called Coulomb's force or Coulomb's interaction. According to Shao et al., 2017, the primary mechanisms for the adsorption of cationic dyes were complexation and electrostatic attractions between the oxygen-containing functional groups of the chemically modified adsorbent and the dye molecules. In the process of methylene blue (MB) adsorption onto biochar, MB is a well-known cationic and primary thiazine dye, while the biochar surface after KOH treatment is enriched with oxygen-containing functional groups (-OH, -COOH) and residual alkaline salts (K_2CO_3, KOH), which typically make the surface negatively charged in neutral to alkaline conditions and have a good adsorption performance for positive ions.

Methylene Blue (MB) is an aromatic heterocyclic basic dye enriched in π-electrons, whose conjugated aromatic rings enable π–π stacking interactions with the polyaromatic carbon structures of biochar formed during pyrolysis and exhibit increased aromaticity and graphitic content (Bollinger et al., 2025; Yu et al., 2024b; Chistie et al., 2025b). The biochar formed from lignocellulosic-rich feedstock has a stronger π–π stacking interaction with MB because its aromatic structure is more durable (Hu et al., 2024b; Hou et al., 2023). Experimental data indicating that biochar with more aromaticity could reach an MB adsorption capacity of more than 150 mg/g also supports the concept that π–π stacking is the main driving force for adsorption (Kataya et al., 2025).

Similarly, the cation-π interaction is a stabilizing electrostatic interaction of a cation with the polarizable π-electron cloud of an aromatic ring (Dougherty, 2025b), where positively charged MB^+ ions are attracted to π-electron-rich regions of aromatic carbon. It has also been acknowledged as a significant noncovalent force in the adsorption process. (Infield et al., 2021b; Kataya et al., 2025).

Compared to traditional methods of physical activation, activation based on KOH offers a unique advantage in terms of building pore structure as well as expanding available surface area, yielding better textural properties (Jedynak & Charmas, 2023). The development of many micropores and mesopores not only expands the available surface area but also makes it simpler for a network of interconnected pores to form. This structural enhancement directly improves the adsorption performance, making it possible for the material to effectively capture a wide range of contaminants such as heavy metals, organic dyes, and gases (e.g., CO_2, H_2, CH_4) (Jedynak & Charmas, 2023;

Zhao et al., 2020). Demonstrating that the treatment of biomass carbon with KOH enhances its specific surface area (SSA) with a large pore volume, multilevel porosity and enhances its performance in a variety of applications (Chang et al., 2025).

4. CONCLUSION

This study has demonstrated that durian husks can be effectively valorized into biochar through saponification pretreatment combined with pyrolysis. The results indicated that pyrolysis at 600 °C for 5 hours significantly enhanced the adsorption performance, particularly when coupled with KOH pretreatment, which exhibited notable adsorption capacity and methylene blue removal efficiency. Compared with the non-pretreated biochar, the treated material showed a larger surface area, higher CEC, and more abundant surface functional groups, all of which contributed to its improved adsorption behavior. Moreover, the adsorption kinetics were better described by the PFO model for the untreated biochar and by the pseudo-second-order model for the pretreated one, while the Freundlich isotherm provided the best fit for the equilibrium data, reflecting the heterogeneous surface characteristics. These findings highlight the dual benefits of converting agricultural residues into high-value adsorbents: addressing waste management challenges and providing a sustainable, low-cost, and environmentally friendly material for wastewater treatment. Future studies may extend this approach to other pollutants and investigate the regeneration and reuse of modified biochar to further assess its practical applicability.

Acknowledgements: *This research was funded by Ho Chi Minh City University of Technology (HCMUT), Vietnam National University under project number of SVOISPL-2024-MT&TN - 49*■

REFERENCES

[1] Katheresan, V., Kansedo, J., & Lau, S. Y. (2018). Efficiency of various recent wastewater dye removal methods: A review. Journal of Environmental Chemical Engineering, 6(4), 4676–4697. https://doi.org/10.1016/j.jece.2018.06.060

[2] Doan, V. T., Le, C. C., Le, H. V. T., Trieu, N. A., Vo, P. L., Tran, D. A., Nguyen, H. V., Tabata, T., & Vu, T. T. H. (2025). Comprehensive Statistical Analysis for Characterizing Water Quality Assessment in the Mekong Delta: Trends, Variability, and Key Influencing Factors. Sustainability, 17(12), 5375. https://doi.org/10.3390/su17125375

[3] Xu, G., Lv, Y., Sun, J., Shao, H., & Wei, L. (2012). Recent advances in biochar applications in agricultural soils: benefits and environmental implications. CLEAN - Soil Air Water, 40(10), 1093–1098. https://doi.org/10.1002/clen.201100738

[4] Sakhiya, A. K., Anand, A., & Kaushal, P. (2020b). Production, activation, and applications of biochar in recent times. Biochar, 2(3), 253–285. https://doi.org/10.1007/s42773-020-00047-1

[5] Ravindiran, G., Rajamanickam, S., Janardhan, G. et al. Production and modifications of biochar to engineered materials and its application for environmental sustainability: a review. Biochar 6, 62 (2024). https://doi.org/10.1007/s42773-024-00350-1

[6] Oliveira, F. R., Patel, A. K., Jaisi, D. P., Adhikari, S., Lu, H., & Khanal, S. K. (2017). Environmental application of biochar: Current status and perspectives. Bioresource technology, 246, 110–122. https://doi.org/10.1016/j.biortech.2017.08.122

[7] Raj, A., Yadav, A., Arya, S., Sirohi, R., Kumar, S., Rawat, A. P., Thakur, R. S., Patel, D. K., Bahadur, L., & Pandey, A. (2021b). Preparation, characterization and agri applications of biochar produced by pyrolysis of sewage sludge at different temperatures. The Science of the Total Environment, 795, 148722. https://doi.org/10.1016/j.scitotenv.2021.148722

[8] Zhang, P., Li, Y., Cao, Y., & Han, L. (2019b). Characteristics of tetracycline adsorption by cow manure biochar prepared at different pyrolysis temperatures. Bioresource Technology, 285, 121348. https://doi.org/10.1016/j.biortech.2019.121348

[9] Zhang, G., Zhang, Q., Sun, K., Liu, X., Zheng, W., & Zhao, Y. (2011). Sorption of simazine to corn straw biochars prepared at different pyrolytic temperatures. Environmental Pollution, 159(10), 2594–2601. https://doi.org/10.1016/j.envpol.2011.06.012

[10] Yaseen, D. A., & Scholz, M. (2018). Textile dye wastewater characteristics and constituents of synthetic effluents: a critical review. International Journal of Environmental Science and Technology, 16(2), 1193–1226. https://doi.org/10.1007/s13762-018-2130-z

[11] Olivito, F., Algieri, V., Jiritano, A., Tallarida, M., Tursi, A., Costanzo, P., Maiuolo, L., & De Nino, A. (2021). Cellulose citrate: a convenient and reusable bio-adsorbent for effective removal of methylene blue dye from artificially contaminated water. RSC Advances, 11, 34309 - 34318. https://doi.org/10.1039/d1ra05464c.

[12] Malatji, N., Makhado, E., Modibane, K., Ramohlola, K., Maponya, T., Monama, G., & Hato, M. (2021). Removal of methylene blue from wastewater using hydrogel nanocomposites: A review. Nanomaterials and Nanotechnology, 11. https://doi.org/10.1177/18479804211039425.

[13] Kurniawan, T., Mengting, Z., Fu, D., Yeap, S., Othman, M., Avtar, R., & Ouyang, T. (2020). Functionalizing TiO2 with graphene oxide for enhancing photocatalytic degradation of methylene blue (MB) in contaminated wastewater.. Journal of environmental management, 270, 110871 . https://doi.org/10.1016/j.jenvman.2020.110871.

[14] Oladoye, P. O., Ajiboye, T. O., Omotola, E. O., & Oyewola, O. J. (2022). Methylene blue dye: Toxicity and potential elimination technology from wastewater.

Results in Engineering, 16, 100678. https://doi.org/10.1016/j.rineng.2022.100678

[15] Khanh, V. K. (2025, July 7). Durian husk – an untapped "gold mine". One World. Retrieved from https://1thegioi.vn/vo-sau-rieng-mo-vang-chua-duoc-quan-tam-dung-muc-234621.html

[16] Shahinyan, G. A., Amirbekyan, A. Y., & Markarian, S. A. (2019). Photophysical properties of methylene blue in water and in aqueous solutions of dimethylsulfoxide. Spectrochimica Acta Part a Molecular and Biomolecular Spectroscopy, 217, 170–175. https://doi.org/10.1016/j.saa.2019.03.079

[17] Kim, W., Shim, T., Kim, Y., Hyun, S., Ryu, C., Park, Y., & Jung, J. (2013). Characterization of cadmium removal from aqueous solution by biochar produced from a giant Miscanthus at different pyrolytic temperatures. Bioresource Technology, 138, 266–270. https://doi.org/10.1016/j.biortech.2013.03.186

[18] Li, M., Liu, Q., Guo, L., Zhang, Y., Lou, Z., Wang, Y., & Qian, G. (2012). Cu(II) removal from aqueous solution by Spartina alterniflora derived biochar. Bioresource Technology, 141, 83–88. https://doi.org/10.1016/j.biortech.2012.12.096

[19] Lee, Y., Park, J., Ryu, C., Gang, K. S., Yang, W., Park, Y., Jung, J., & Hyun, S. (2013). Comparison of biochar properties from biomass residues produced by slow pyrolysis at 500°C. Bioresource Technology, 148, 196–201. https://doi.org/10.1016/j.biortech.2013.08.135

[20] Jeong, C. Y., Dodla, S. K., & Wang, J. J. (2015). Fundamental and molecular composition characteristics of biochars produced from sugarcane and rice crop residues and by-products. Chemosphere, 142, 4–13. https://doi.org/10.1016/j.chemosphere.2015.05.084

[21] Sun, J., He, F., Pan, Y., & Zhang, Z. (2016). Effects of pyrolysis temperature and residence time on physicochemical properties of different biochar types. Acta Agriculturae Scandinavica, Section B — Soil & Plant Science, 67(1), 12–22. https://doi.org/10.1080/09064710.2016.1214745

[22] Wahyu, M. E., Damayanti, D., & Wu, H. S. (2025). Production, Characterization, and Application of KOH-Activated Biochar from Rice Straw for Azo Dye Adsorption. Biomass, 5(3), 40. https://doi.org/10.3390/biomass5030040

[23] Nguyen, L. X., My, P. T., DO, Nguyen, C. H., Kose, R., Okayama, T., Pham, T. N., Nguyen, P. D., & Miyanishi, T. (2018). Properties of Biochars Prepared from Local Biomass in the Mekong Delta, Vietnam. BioResources, 13(4). https://doi.org/10.15376/biores.13.4.7325-7344

[24] Gurav, R., Bhatia, S. K., Choi, T., Choi, Y., Kim, H. J., Song, H., Lee, S. M., Park, S. L., Lee, H. S., Koh, J., Jeon, J., Yoon, J., & Yang, Y. (2020). Application of macroalgal biomass derived biochar and bioelectrochemical system with Shewanella for the adsorptive removal and biodegradation of toxic azo dye. Chemosphere, 264, 128539. https://doi.org/10.1016/j.chemosphere.2020.128539

[25] Jedynak, K., & Charmas, B. (2023c). Adsorption properties of biochars obtained by KOH activation. Adsorption, 30(2), 167–183. https://doi.org/10.1007/s10450-023-00399-7

[26] Shao, H., Li, Y., Zheng, L., Chen, T., & Liu, J. (2017). Removal of methylene blue by chemically modified defatted brown algae Laminaria japonica. Journal of the Taiwan Institute of Chemical Engineers, 80, 525–532. https://doi.org/10.1016/j.jtice.2017.08.023

[27] Bollinger, JC., Lima, E.C., Mouni, L. et al. Molecular properties of methylene blue, a common probe in sorption and degradation studies: a review. Environ Chem Lett 23, 1403–1424 (2025). https://doi.org/10.1007/s10311-025-01856-1

[28] Yu, H., Zhang, Y., Wang, L., Tuo, Y., Yan, S., Ma, J., Zhang, X., Shen, Y., Guo, H., & Han, L. (2024b). Experimental and DFT insights into the adsorption mechanism of methylene blue by alkali-modified corn straw biochar. RSC Advances, 14(3), 1854–1865. https://doi.org/10.1039/d3ra05964b

[29] Chistie, S. M., Naik, S. U., Rajendra, P., Apeksha, N., Mishra, R. K., Albasher, G., Chinnam, S., Jeppu, G. P., Arif, Z., & Hameed, J. (2025b). Production and characterization of magnetic Biochar derived from pyrolysis of waste areca nut husk for removal of methylene blue dye from wastewater. Scientific Reports, 15(1). https://doi.org/10.1038/s41598-025-03359-z

[30] Hu, M., Chen, J., & Liu, Y. (2024b). Structural properties and adsorption performance relationship towards three categories of lignin and their derived biochar. Bioresource Technology, 401, 130712. https://doi.org/10.1016/j.biortech.2024.130712

[31] Hou, M., He, Y., Yang, X., Yang, Y., Lin, X., Feng, Y., Kan, H., Hu, H., He, X., & Liu, C. (2023). Preparation of Biomass Biochar with Components of Similar Proportions and Its Methylene Blue Adsorption. Molecules, 28(17), 6261. https://doi.org/10.3390/molecules28176261

[32] Kataya, G., Issa, M., Badran, A., Cornu, D., Bechelany, M., Jellali, S., Jeguirim, M., & Hijazi, A. (2025). Dynamic removal of methylene blue and methyl orange from water using biochar derived from kitchen waste. Scientific reports, 15(1), 29907. https://doi.org/10.1038/s41598-025-14133-6

[33] Dougherty, D. A. (2025b). The Cation−π Interaction in Chemistry and Biology. Chemical Reviews. https://doi.org/10.1021/acs.chemrev.4c00707

[34] Infield, D. T., Rasouli, A., Galles, G. D., Chipot, C., Tajkhorshid, E., & Ahern, C. A. (2021b). Cation-π Interactions and their Functional Roles in Membrane Proteins. Journal of Molecular Biology, 433(17), 167035. https://doi.org/10.1016/j.jmb.2021.167035

[35] Jedynak, K., Charmas, B. Adsorption properties of biochars obtained by KOH activation. Adsorption 30, 167–183 (2024). https://doi.org/10.1007/s10450-023-00399-7

[36] Chang, S., Wang, L., & Yao, L. (2025). Properties of Sunflower Straw Biochar Activated Using Potassium Hydroxide. Molecules, 30(6), 1332. https://doi.org/10.3390/molecules30061332